ADVANCED MATERIALS
www.advmat.de

Low-Power, Electrochemically Tunable Graphene Synapses for Neuromorphic Computing

*Mohammad Taghi Sharbati, Yanhao Du, Jorge Torres, Nolan D. Ardolino, Minhee Yun, and Feng Xiong**

Brain-inspired neuromorphic computing has the potential to revolutionize the current computing paradigm with its massive parallelism and potentially low power consumption. However, the existing approaches of using digital complementary metal–oxide–semiconductor devices (with "0" and "1" states) to emulate gradual/analog behaviors in the neural network are energy intensive and unsustainable; furthermore, emerging memristor devices still face challenges such as nonlinearities and large write noise. Here, an electrochemical graphene synapse, where the electrical conductance of graphene is reversibly modulated by the concentration of Li ions between the layers of graphene is presented. This fundamentally different mechanism allows to achieve a good energy efficiency (<500 f) per switching event), analog tunability (>250 nonvolatile states), good endurance, and retention performances, and a linear and symmetric resistance response. Essential neuronal functions such as excitatory and inhibitory synapses, long-term potentiation and depression, and spike timing dependent plasticity with good repeatability are demonstrated. The scaling study suggests that this simple, two-dimensional synapse is scalable in terms of switching energy and speed.

Unlike modern computers that use digital "0" and "1" states for computation, neural networks in the human brain exhibit analog changes in neural connections (i.e., synaptic weight) during decision-making and learning processes.[1,2] This analog nature as well as the neural network's massive parallelism are partly why human brains (≈20 W) are much better at complex tasks such as pattern recognition than even the most powerful computers (≈1 MW) with significantly better energy efficiency.[1,2] The field of neuromorphic computing—emulating the brain with computational hardware—can have a profound impact in next-generation computing and artificial intelligence.

The neural network in a human brain has $\approx 10^{11}$ neurons. Each neuron is typically connected to ≈5,000 to 10,000 other neurons through synapses, creating a dense neural network.[2] The weight/conductance of a synapse determines the strength of the connection between two neurons, as illustrated in **Figure 1**a. This synaptic weight can be altered in small increments by neuronal activities through a process called synaptic plasticity,[3] which is widely believed to be responsible for the learning process in the brain. Researchers have been striving to emulate the brain through various aspects of computing, such as algorithms (cognitive functions),[4] architectures (neural networks),[5] and devices (neurons and synapses).[6] At the device level, synapses are still implemented by dozens of digital complementary metal–oxide–semiconductor (CMOS) devices in today's artificial neural networks,[5,6] and these devices cannot truly simulate the analog behaviors of biological synapses. Thus, the energy consumption under the current approaches will be astronomically high if these systems are scaled to the same level of complexity as the human brain ($\approx 10^{11}$ neurons and $\approx 10^{15}$ synapses).

Emerging memory devices such as phase-change memory[7] (PCM), oxide-based resistive random-access memory[8] (RRAM), and metal ion based electrochemical metallization memory[9,10] (ECM) devices have been studied to mimic synaptic connections through their programmable device conductance. While these emerging technologies offer promising aspects such as analog conductance, good scalability, high switching speeds, and simple structures, there are still major hurdles that must be overcome before they can satisfy the performance requirements of a neural architecture. Specifically, the high programming power and poor reliability issues of PCMs need to be mitigated,[1,11] while RRAMs and ECMs still suffer from large temporal (cycle-to-cycle) and spatial (device-to-device) variabilities as well as nonlinear characteristics.[2,10,12] Other novel approaches involving two-dimensional (2D) materials[13] or epitaxial SiGe[14] have demonstrated encouraging proof-of-concept performances. However, an artificial synapse that fulfills all the desired traits for neuromorphic applications has not yet been demonstrated.

Recently, electrochemical devices have been proposed as an alternative approach to synaptic electronics. In 2017, Fuller et al.[15] developed a $Li_{1-x}CoO_2$ synaptic transistor based on Li intercalation, while van de Burgt et al.[16] demonstrated an organic electrochemical synaptic device with a low programming power and good retention. These pioneering works illustrate the feasibility of engineering the device resistance through controlled electrochemical reactions for analog memory applications.

M. T. Sharbati, Y. Du, J. Torres, N. D. Ardolino, Prof. M. Yun, Prof. F. Xiong
Department of Electrical and Computer Engineering
The University of Pittsburgh
Pittsburgh, PA 15261, USA
E-mail: f.xiong@pitt.edu

The ORCID identification number(s) for the author(s) of this article can be found under https://doi.org/10.1002/adma.201802353.

DOI: 10.1002/adma.201802353

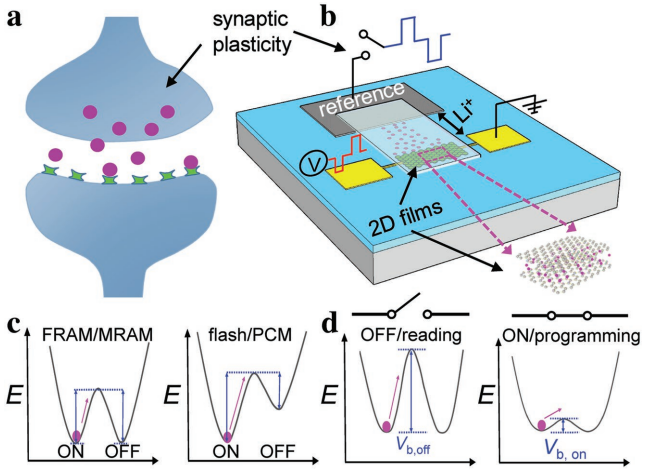

Figure 1. Electrochemical graphene synapse. a) Schematic of a biological synapse. b) Schematic of our graphene synapse. The synaptic weight is encoded into the channel conductance of the graphene device. We can modulate the synaptic weight (channel conductance) in our device by adjusting the Li ion concentration between graphene layers via electrochemical intercalation. c) Schematic of conventional memory technologies, where the energy barriers for programming and retention are the same, thereby creating a tradeoff between low-power programming writing and good retention. d) Schematics of the energy barriers for our electrochemical synapse during retention (read) and programming (write). The retention and programming mechanisms are decoupled through a circuit switch. The high $V_{b,\,off}$ barrier during the open circuit read operation ensures good retention, while the low $V_{b,\,on}$ barrier during the closed circuit write operation allows low-power programming.

Here, we present an electrochemical graphene synapse with a low power consumption (<500 fJ per switching event), precise and reversible control over the resistance (<0.4% step change per synaptic event), a linear and symmetric resistance response, good endurance and retention behaviors, and a potential for scaling in switching speed and energy. The 2D nature of graphene makes it an excellent host for accommodating guest ions between its layers.[17] We choose to intercalate Li ions in few-layer graphene in this work because (1) the electrochemical behaviors of graphite with Li ions have been thoroughly characterized since this material has already been widely used as an anode in Li-ion batteries (LIBs);[17–19] and (2) Li ions have been reported to have an unusually high diffusion coefficient (7×10^{-5} cm^2 s^{-1}) in bilayer graphene at room temperature,[20] suggesting that a fast switching speed is possible. While Li ions can potentially be a source of contamination for Si devices[21] if not handled and contained properly, it is a good material to start with for our proof-of-concept demonstration because of its well-known electrochemical behaviors. In addition to graphene's compatibility with the CMOS technology (good thermal stability and 2D nature)[22] and its potential for application in flexible electronics (excellent mechanical properties and ultrathin layers),[23] graphene can be easily integrated with emerging 2D electronics to form a densely connected logic and memory network, enabling a new paradigm in computing architectures and breaking the existing "memory bottleneck".

Schematics of a biological synapse and our electrochemical graphene synapse are illustrated in Figure 1a,b, where the graphene channel conductance represents the synaptic weight, and the weight of the graphene synapse can be modulated by the signal from the reference electrode (lithium ion phosphate, or LFP), representing signals from presynaptic neurons. The solid electrolyte ($LiClO_4$ in poly(ethylene oxide) (PEO), see Supporting Information) allows ionic exchange to occur between graphene and LFP. A major advantage of this electrochemical approach is that we can achieve the reversible and precise tuning of the graphene device conductance by controlling the concentration of Li ions in graphene[17,18] to mimic synaptic plasticity. In addition, unlike conventional memory technologies, the programming and storage mechanisms in the electrochemical synapse are decoupled,[16] allowing us to achieve both low-power switching and good retention properties. Figure 1c shows a schematic of the energy barriers for typical thermodynamic memory (ferroelectric and resistive random-access)[24] and kinetic memory (flash and PCM)[25] devices. The barrier heights for these memory devices are the same during the write and read operations, imposing a tradeoff between a low programming power (write) and good retention (read) in conventional memory technologies. In our electrochemical device, the programming (write) and retention (read) barriers can be decoupled by a circuit switch between graphene and LFP (Figure 1d). During the write operation, the circuit is closed, which allows both electrons (through the external circuit) and ions (through the electrolyte) to be exchanged between graphene and the reference electrode under a small bias. During the read operation, where the graphene resistance is sensed by a low-voltage pulse across the graphene channel with the circuit between graphene and LFP open, the electron-blocking electrolyte prevents any electrochemical reactions and therefore maintains the state of the graphene synapse.

Electrochemical intercalation has been the cornerstone of the LIB industry for decades, but it has only recently been employed as a technique for engineering the properties of 2D materials through charge transfer, impurity scattering, and band gap engineering.[26] To lower the resistance of the graphene synapse through intercalation (**Figure 2**a), we used an external current to drive both negatively charged electrons and positively charged Li^+ ions from the reference electrode (LFP) to graphene. When we reversed the polarity of the external current, Li ions was driven out of the graphene (deintercalation), and the graphene resistance was increased. Governed by charge neutrality, for every electron, e^-, flowing into/out of graphene in the external circuit, a corresponding Li^+ ion enters/leaves graphene through the electrolyte. This process allows us to precisely modulate the Li ion concentration in our graphene synapse (thus, its synaptic weight) by controlling the total amount of charge (= current × time) transferred into/out of the graphene.

Figure 2b shows the galvanostatic discharge measurement of a 20 nm graphite (see Figure 2d inset) thin film during Li intercalation. The intercalation process was controlled by a BioLogic SP-200 electrochemical workstation, and the discharge current was kept at 100 pA. We monitored the electrochemical potential of graphene by measuring the voltage difference between graphene and the reference LFP electrode. We observed multiple plateaus in our measurement, which corresponded to the formation of the intermediate compounds LiC_{72}, LiC_{36}, LiC_{18}, LiC_{12}, and, lastly, the stoichiometric limit LiC_6, consistent with similar measurements reported in the literature.[17,18,27] Even though intercalation is initiated from the edges of the 2D

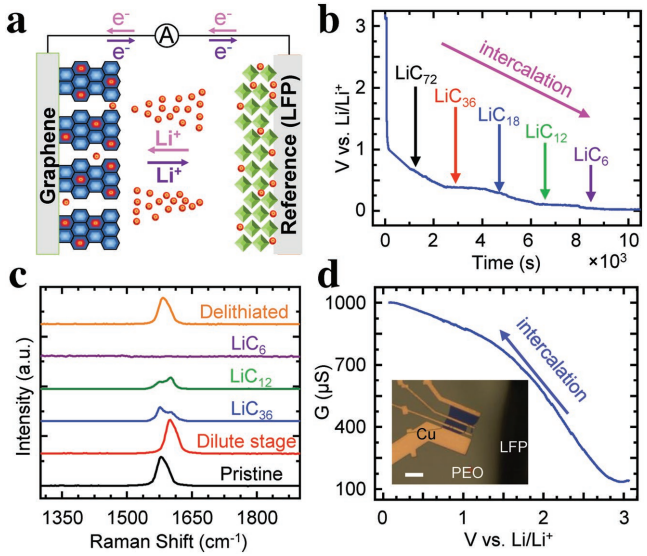

Figure 2. Electrochemical Li intercalation in graphene. a) Schematic of the reversible electrochemical Li intercalation process. The pink (purple) arrows indicate the intercalation (deintercalation) process, where both electrons, e^-, and Li^+ ions flow into (out of) the graphene working electrode. b) The galvanostatic discharge process of graphene. The plateaus indicate various intermediate graphene intercalation compounds. c) In situ Raman spectra of different intermediate graphene intercalation compounds. d) Modulation of the graphene conductance (synaptic weight) as a function of its electrochemical potential (Li concentration). The inset shows an optical image of the graphene synapse. The scale bar is 20 μm.

crystal,[28] previous kinetics studies[18,29] have shown that all of the intermediate intercalated compounds (e.g., LiC_{72}) have an approximately uniform distribution of intercalant (Li). This has been attributed to the formation and rapid growth of the intercalate nucleus.[18,29] This is advantageous for the development of graphene synapse since it ensures that graphene devices with similar dimensions will have the same electrochemical response when they are intercalated to the same stage.

We also performed in situ Raman measurements (Horiba with a 532 nm laser) to examine the different stages of graphene intercalation compounds, as illustrated in Figure 2c. Our pristine graphene displayed good film quality with no D band. Upon Li intercalation, we first noticed a slight upshift of the G band from 1580 to 1605 cm^{-1}, which was likely due to the doping effect of Li intercalation.[27,28,30] Subsequently, the G band split into two peaks, which was possibly due to a weakening of the C−C bond upon the influx of Li ions.[27,30] Eventually, the G band vanished into the background noise at the LiC_6 stage. The G band reappeared upon deintercalation, thereby confirming the reversible nature of the electrochemical process. We performed direct current measurements (Figure 2d) to measure the electrical conductance of graphene as a function of its Li content, i.e., electrochemical potential. We observed an ≈700% modulation in the synaptic weight (channel resistance) in our graphene synapse, which is significantly more than the ≈150% change that occurs in biological synapses.[3b] This large modulation in electrical conductance suggests that the electrical characteristics of the graphene electrochemical synapse is mostly dominated by the electrochemical state (i.e., Li concentration) of the device, hence making our electrochemical synapse more immune to the variabilities of graphene devices from the growth and/or fabrication processes and suitable for scaling up to dense neural networks. Looking into the future, our electrochemical synapse's tolerance for device-to-device variation in graphene will allow us to adopt the high-throughput, large-area chemical vapor deposition growth of graphene thin films[31] for array-level integrations.

We could mimic both synaptic potentiation and depression with our 2D electrochemical synapse, as illustrated in **Figure 3**a,b, respectively. When we sent a single intercalation current pulse (50 pA, 10 ms) to a 8 nm thick graphene synapse (see Figure S1, Supporting Information) to emulate a presynaptic input, we observed an ≈30 Ω (0. 67%) decrease in the channel resistance R, which mimics an increase in the synaptic weight of an excitatory synapse upon stimulation.[3b,32] The ΔR value gradually diminished to a stable value of $\Delta R' = -10$ Ω (−0.22%). This result is similar to the short-term potentiation effect in a neural network, where the synaptic strength changes upon initial stimulation. This learning effect (increase in synaptic weight) gradually fades over time but still results in a permanent, smaller change in the synaptic strength.[3c]

Physically, the initial large change in the channel conductance of graphene likely results from a combination of the doping effect of Li intercalation[28] and the electric double layer (EDL) gating effect[33] from the intercalation pulse. The EDL gating effect, which originates from the introduction of a large amount of charge at the graphene/electrolyte interface by the applied voltage, is capacitive in nature and thus dissipates[33]

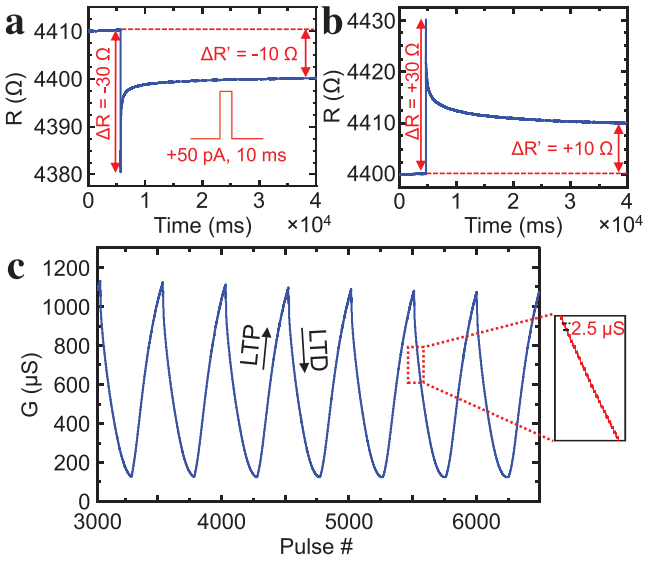

Figure 3. Synaptic plasticity. Potentiation a) and depression b) behaviors of an electrochemical graphene synapse. The decrease (increase) in the channel resistance of graphene upon an intercalation (deintercalation) pulse (50 pA, 10 ms) mimics a potentiation (depression) synaptic response. c) Demonstration of long-term potentiation (LTP) and depression (LTD) in our 2D synapse through controlled intercalation. We programmed >250 distinct states into our electrochemical synapse through a series of intercalation/deintercalation pulses. The synaptic response is symmetric, linear, and repeatable.

when the applied pulse is off. The doping effect of Li intercalation is nonvolatile[28] and contributes to the lasting increase in the channel conductance. Figure 3b shows synaptic depression, where the synaptic weight (channel conductance) decreases upon presynaptic stimulation (deintercalation pulse). Similarly, we observed a large initial increase ($\Delta R = +30\ \Omega$) in the channel resistance, which settled down to a stable value at $\Delta R' = +10\ \Omega$, representing the nonvolatile effect from Li deintercalation.

Long-term potentiation (LTP) and depression (LTD), where the synaptic strength can be permanently improved and diminished through repeated stimulation, are two essential neuronal functions in learning.[34] In Figure 3c, we demonstrated the occurrence of LTP and LTD in our 2D electrochemical synapse through the application of a series of intercalation and deintercalation pulses (50 pA, 10 ms). We were able to program over >250 distinct states into our device, suggesting that an extremely large number of nonvolatile states are available for computations in our synapse. The synaptic response was linear and reproducible, which is desirable for system-level integration.[6] The *R*-squared value of the linear fit of the conductance response between 10% to 90% lithiation stage is 0.994, indicating a good linearity of the conductance response. This is expected because the increase in conductance depends on the amount of charge transferred into (out of) the graphene through the intercalation (deintercalation) pulse.[16] This relationship is evident in our results, where the change in channel conductance, ΔG is linearly dependent on the amplitude of the applied pulse (see Figure S4, Supporting Information). This result suggests that we can further refine the step size (ΔG) and increase the memory density in our electrochemical synapse by modulating the amplitude of the applied pulses.

The graphene synapse displays good retention and endurance behaviors. The device conductance was stable under a 0.1 V reading bias (across the graphene channel) for more than 13 h (see Figure S5, Supporting Information). We measured a 3.2% decrease in conductance at the end of the 13 h stress test, consistent with the self-discharge effect observed in LIBs, where the conductance of the fully charged batteries typically decreases by ≈3–5% in the first 24 h.[35] While this conductance drift is less than ideal for long term retention, it may be mitigated by adding a thin passivation layer on graphene, as it has been employed to reduce the self-discharge rate in LIBs.[36] Furthermore, this self-discharge rate in LIBs drastically slows down to ≈1–2% per month thereafter,[37] projecting potentially good long-term retention properties for the graphene synapse. We cycled our device between its two intermediate states for 500 cycles (see Figure S6, Supporting Information) and observed small cycle-to-cycle variations, demonstrating an excellent reliability performance.

Spike timing dependent plasticity (STDP) plays an important role in learning and memory in biological neural networks.[3c] As illustrated in different forms of STDP shown in **Figure 4**a, an STDP scheme governs how the spike (presynaptic signal) timing difference (Δt) determines the amplitude of the change in the synaptic weight (Δw).[1] We demonstrated the STDP capability in our electrochemical synapse through a two-pulse programming scheme. As shown in Figure 4b, when the timing difference between the two intercalation pulses was small, we observed a large increase in the channel conductance (ΔG), similar to the strong memory effect observed for two temporally close events. When the timing difference was large, the change in channel conductance was subsequently smaller, analogous to the scenario in which the reinforcing memory effect is weak when two events are temporally far apart.

Interestingly, the conductance change, ΔG, followed an exponentially decaying trend with three characteristic time constants, τ_1 = 22 ms, τ_2 = 315 ms, and τ_3 = 19 s, similar to the timescale of biological synapses.[32] We speculate that the smaller time constants (τ_1 and τ_2) are related to the diffusion process during intercalation and thus should depend on the dimension (width and length) of the graphene synapse. The third (and much larger) time constant (τ_3), which may rise from the diffusion process from LFP to graphene, is needed to better fit the tail end of the decay, as we illustrated in Figure S7 of the Supporting Information. Using a diffusion coefficient, *D*, of $\approx 4 \times 10^{-6}$ cm^2 s^{-1} for Li ions in graphene[20] and lateral dimensions of 4 µm (width) and 15 µm (length) for the graphene device, we estimated the average diffusion time ($\tau_D \approx L^2/2D$) for our electrochemical synapse to be ≈20 and 280 ms in the width and length directions, respectively, consistent with our measured time constants (22 and 315 ms). These result are

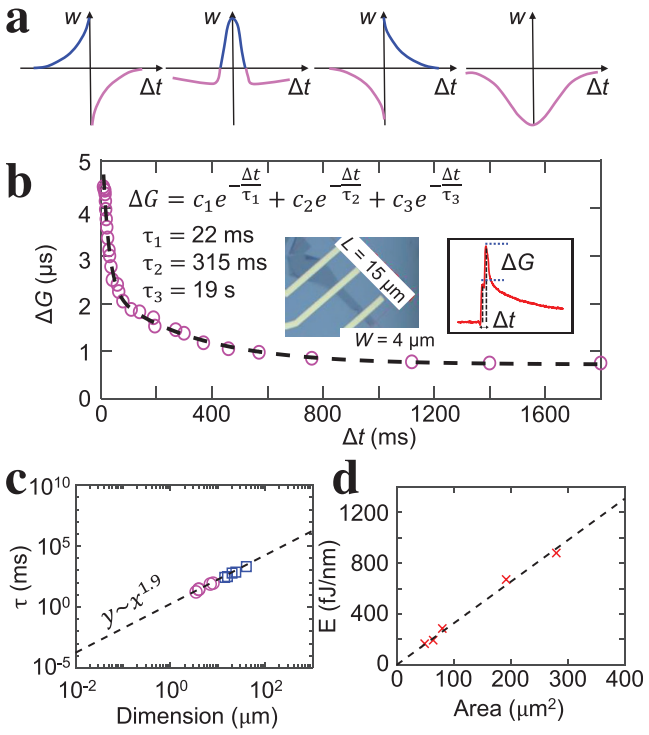

Figure 4. Spike timing dependent plasticity (STDP). a) Different forms of STDP in biological synapses, where the change in synaptic weight (w) depends on the timing difference (Δt) of synaptic events. b) In our graphene synapse, the change in resistance (synaptic weight) depends on the timing difference between programming pulses, mimicking the STDP scheme. The time constants τ_1, τ_2, and τ_3 are ≈22 ms, 315 ms, and 19 s, similar to biological synapses. The ratio of the time constants $\tau_2/\tau_1 = 14.5$ is similar to the ratio of length/width for graphene $(L/W)^2 = 14.1$, as predicted by the Einstein diffusion equation $\tau_D \approx L^2/(2D)$. c) Scaling trend of STDP time constants τ_1 (pink circle) and τ_2 (blue square) as a function of device dimension (W or L). d) Scaling trend of switching energy (normalized by thickness) as a function of flake area.

consistent with switching times reported by van de Burgt et al. for the organic electrochemical synapses[16] and suggest that we can engineer and optimize the timing of the STDP for our 2D electrochemical synapse by altering the device geometry.

We studied the scalability of our 2D electrochemical synapse over a wide range of dimensions. The size and geometry of the graphene synapse determine the density of our analog memory as well as the programming speed and energy. As illustrated in Figure 4c, the time constants for STDP in our graphene synapse exhibited a power law dependence ($\gamma = cx^{\alpha}$ with $\alpha = 1.9$) over the device dimensions, as governed by Einstein's diffusion equation, $\tau_D \approx L^2/2D$. We project that the diffusion time for a graphene flake with 30 nm × 30 nm lateral dimensions can be as fast as ≈100 ns (10 MHz), which is comparable to that of dynamic random-access memory devices.[38]

We also plotted the switching energy (normalized to the thickness) needed to induce a 0.4% change in the graphene synapse as a function of the area of the flake in Figure 4d. The switching energy ($E = I \times V \times t$) depends on the programming voltage (V) and the amount of charge ($I \times t$) transferred. The programming voltage is determined by the electrochemical potential of graphene and remains approximately constant. The total charge should scale linearly with the area of the flake (assuming uniform thickness). The linear dependence of E on the area confirms our analysis and suggests an excellent scaling potential of the electrochemical synapse. The switching energy per synaptic event for our smallest device (3 μm × 12 μm × 3 nm) is 500 fJ, comparable to the switching energy of a biological synapse. We project that the switching energy of a submicron device (30 nm × 30 nm × 1 nm) can be as low as ≈4 aJ, which is several orders of magnitude lower than the switching energy of biological synapses[3b] and will significantly improve the energy efficiency of artificial neural networks.

In conclusion, we developed a novel 2D electrochemical device as an artificial synapse. Our graphene synapse displayed an energy efficiency ≈500 fJ per switching, analog tunability (>250 distinct states), a linear and symmetrical response, and good retention and endurance performances. We demonstrated basic neuronal functions, such as short-term and long-term potentiation/depression as well as STDP. Our graphene synapse also exhibited potential for scaling, where we project a nanoscale electrochemical synapse can operate with as low of a switching energy as 4 aJ per switching event at 10 MHz. With graphene's 2D flexible nature and CMOS compatibility, our electrochemical synapse provides exciting opportunities to realize the hardware implementation of fully functioning artificial neural network for neuromorphic computing.

Experimental Section

Device Fabrication: Graphene flakes were obtained through mechanical exfoliation and transferred onto SiO_2 (285 nm) on Si substrate. Electron-beam (e-beam) lithography was performed to define the metal contacts –80 nm Cu, which was deposited through e-beam evaporation. All devices were annealed under forming gas flow (Ar/N_2) at 300 °C for an hour to improve contact resistance and remove tape residues and other surface adsorbents. Upon applying the electrolyte ($LiClO_4$ in PEO) and the reference electrode (LFP) (see Supporting Information for more details), the devices were further annealed at 80 °C in vacuum (≈10^{-5} Torr) for two hours to eliminate the residual moisture in the electrolyte.

Electrical and Electrochemical Characterization: Electrochemical characterizations were carried out with an SP-200 BioLogic workstation. During galvanostatic discharge measurements, a constant 100 pA charging/discharging current was applied with the graphene connected to the working electrode and the LFP connected to the counter/reference electrodes. Electrical and pulse measurements were performed with a Keithley Semiconductor Parameter Analyzer (4200-SCS) with pulse measuring units. All electrical measurements were performed in a vacuum probe station (≈10^{-5} Torr).

Raman Spectroscopy: Raman spectroscopy was performed using a Horiba LabRam instrument with a 532 nm laser. With a 100× objective, the laser spot radius was ≈300 nm. The absorbed laser power was kept low (<20 μW) to avoid laser heating.

Supporting Information

Supporting Information is available from the Wiley Online Library or from the author.

Acknowledgements

M.T.S., Y.D., and F.X. gratefully acknowledge support from the Electrical and Computer Engineering department, the Swanson School of Engineering, and the Central Research Developmental Fund at University of Pittsburgh. T.J. and M.Y. acknowledge support from the National Science Foundation (ECCS 1709307). The authors thank Dr. Ke Xu and Dr. Yiyang Li for valuable discussions. During review, the authors became aware of work by another group using ionic-gating-modulated WSe_2 as artificial synapse.[39]

Conflict of Interest

The authors declare no conflict of interest.

Keywords

artificial synapse, electrochemical intercalation, graphene, neuromorphic computing

Received: April 12, 2018
Revised: June 14, 2018
Published online: July 23, 2018

[1] D. Kuzum, S. M. Yu, H. S. P. Wong, *Nanotechnology* **2013**, *24*, 382001.
[2] N. K. Upadhyay, S. Joshi, J. J. Yang, *Sci. China Inf. Sci.* **2016**, *59*, 061404.
[3] a) M. V. L. Bennett, R. S. Zukin, *Neuroendocrinology* **2004**, *41*, 495; b) A. E. Pereda, *Nat. Rev. Neurosci.* **2014**, *15*, 250; c) C. Zamarreno-Ramos, L. A. Camunas-Mesa, J. A. Perez-Carrasco, T. Masquelier, T. Serrano-Gotarredona, B. Linares-Barranco, *Front. Neurosci.-Switz.* **2011**, *5*, 1.
[4] H. Markram, *Nat. Rev. Neurosci.* **2006**, *7*, 153.
[5] S. B. Furber, D. R. Lester, L. A. Plana, J. D. Garside, E. Painkras, S. Temple, A. D. Brown, *IEEE Trans. Comput.* **2013**, *62*, 2454.
[6] P. A. Merolla, J. V. Arthur, R. Alvarez-Icaza, A. S. Cassidy, J. Sawada, F. Akopyan, B. L. Jackson, N. Imam, C. Guo, Y. Nakamura, B. Brezzo, I. Vo, S. K. Esser, R. Appuswamy, B. Taba, A. Amir, M. D. Flickner, W. P. Risk, R. Manohar, D. S. Modha, *Science* **2014**, *345*, 668.

[7] a) T. Tuma, A. Pantazi, M. Le Gallo, A. Sebastian, E. Eleftheriou, *Nat. Nanotechnol.* **2016**, *11*, 693; b) G. W. Burr, R. M. Shelby, S. Sidler, C. di Nolfo, J. Jang, I. Boybat, R. S. Shenoy, P. Narayanan, K. Virwani, E. U. Giacometti, B. N. Kurdi, H. Hwang, *IEEE Trans. Electron Dev.* **2015**, *62*, 3498; c) D. Kuzum, R. G. D. Jeyasingh, S. M. Yu, H. S. P. Wong, *IEEE Trans. Electron Dev.* **2012**, *59*, 3489.

[8] a) D. B. Strukov, G. S. Snider, D. R. Stewart, R. S. Williams, *Nature* **2008**, *453*, 80; b) S. M. Yu, Y. Wu, R. Jeyasingh, D. G. Kuzum, H. S. P. Wong, *IEEE Trans. Electron Dev.* **2011**, *58*, 2729; c) J. J. S. Yang, D. B. Strukov, D. R. Stewart, *Nat. Nanotechnol.* **2013**, *8*, 13; d) Z. Wang, S. Joshi, S. Savel'ev, W. Song, R. Midya, Y. Li, M. Rao, P. Yan, S. Asapu, Y. Zhuo, H. Jiang, P. Lin, C. Li, J. H. Yoon, N. K. Upadhyay, J. Zhang, M. Hu, J. P. Strachan, M. Barnell, Q. Wu, H. Wu, R. S. Williams, Q. Xia, J. J. Yang, *Nat. Electron.* **2018**, *1*, 137.

[9] S. La Barbera, D. Vuillaume, F. Alibart, *ACS Nano* **2015**, *9*, 941.

[10] Y. Yang, P. Gao, L. Li, X. Pan, S. Tappertzhofen, S. Choi, R. Waser, I. Valov, W. D. Lu, *Nat. Commun.* **2014**, *5*, 4232.

[11] B. L. Jackson, B. Rajendran, G. S. Corrado, M. Breitwisch, G. W. Burr, R. Cheek, K. Gopalakrishnan, S. Raoux, C. T. Rettner, A. Padilla, A. G. Schrott, R. S. Shenoy, B. N. Kurdi, C. H. Lam, D. S. Modha, *ACM J. Emerging Technol. Comput.* **2013**, *9*, 12.

[12] a) D. S. Jeong, R. Thomas, R. S. Katiyar, J. F. Scott, H. Kohlstedt, A. Petraru, C. S. Hwang, *Rep. Prog. Phys.* **2012**, *75*, 076502; b) D. Ielmini, *Semicond. Sci. Technol.* **2016**, *31*, 063002.

[13] a) H. Tian, Q. S. Guo, Y. J. Xie, H. Zhao, C. Li, J. J. Cha, F. N. Xia, H. Wang, *Adv. Mater.* **2016**, *28*, 4991; b) H. Tian, W. T. Mi, X. F. Wang, H. M. Zhao, Q. Y. Xie, C. Li, Y. X. Li, Y. Yang, T. L. Ren, *Nano Lett.* **2015**, *15*, 8013; c) M. Wang, S. Cai, C. Pan, C. Wang, X. Lian, Y. Zhuo, K. Xu, T. Cao, X. Pan, B. Wang, S.-J. Liang, J. J. Yang, P. Wang, F. Miao, *Nat. Electron.* **2018**, *1*, 130.

[14] S. Choi, S. H. Tan, Z. Li, Y. Kim, C. Choi, P.-Y. Chen, H. Yeon, S. Yu, J. Kim, *Nat. Mater.* **2018**, *17*, 335.

[15] E. J. Fuller, F. El Gabaly, F. Leonard, S. Agarwal, S. J. Plimpton, R. B. Jacobs-Gedrim, C. D. James, M. J. Marinella, A. A. Talin, *Adv Mater* **2017**, *29*, 1604310.

[16] Y. van de Burgt, E. Lubberman, E. J. Fuller, S. T. Keene, G. C. Faria, S. Agarwal, M. J. Marinella, A. A. Talin, A. Salleo, *Nat. Mater.* **2017**, *16*, 414.

[17] W. Z. Bao, J. Y. Wan, X. G. Han, X. H. Cai, H. L. Zhu, D. H. Kim, D. K. Ma, Y. L. Xu, J. N. Munday, H. D. Drew, M. S. Fuhrer, L. B. Hu, *Nat. Commun.* **2014**, *5*, 4224.

[18] M. S. Dresselhaus, G. Dresselhaus, *Adv. Phys.* **1981**, *30*, 139.

[19] M. D. Levi, E. Markevich, A. Aurbach, *J. Phys. Chem. B* **2005**, *109*, 7420.

[20] M. Kuhne, F. Paolucci, J. Popovic, P. M. Ostrovsky, J. Maier, J. H. Smet, *Nat. Nanotechnol.* **2017**, *12*, 895.

[21] V. Gorodokin, D. Zemlyanov, presented at *23rd IEEE Convention of Electrical and Electronics Engineers in Israel*, **2004**, September 6–7.

[22] M. H. Bae, Z. Y. Li, Z. Aksamija, P. N. Martin, F. Xiong, Z. Y. Ong, I. Knezevic, E. Pop, *Nat. Commun.* **2013**, *4*, 1.

[23] H. Jang, Y. J. Park, X. Chen, T. Das, M. S. Kim, J. H. Ahn, *Adv. Mater.* **2016**, *28*, 4184.

[24] S. Kim, S. Choi, W. Lu, *ACS Nano* **2014**, *8*, 2369.

[25] D. Ielmini, A. L. Lacaita, *Mater. Today* **2011**, *14*, 600.

[26] a) G. Zhu, J. Liu, Q. Zheng, R. Zhang, D. Li, D. Banerjee, D. G. Cahill, *Nat. Commun.* **2016**, *7*, 13211; b) J. S. Kang, M. Ke, Y. Hu, *Nano Lett.* **2017**, *17*, 1431; c) A. Sood, F. Xiong, H. Wang, Y. Cui, E. Pop, K. E. Goodson, *MRS Spring Meeting*, MRS, Phoenix, AZ **2017**.

[27] M. Inaba, H. Yoshida, Z. Ogumi, T. Abe, Y. Mizutani, M. Asano, *J. Electrochem. Soc.* **1995**, *142*, 20.

[28] F. Xiong, H. T. Wang, X. G. Liu, J. Sun, M. Brongersma, E. Pop, Y. Cui, *Nano Lett.* **2015**, *15*, 6777.

[29] J. M. Thomas, G. R. Millward, R. F. Schlögl, H. P. Boehm, *Mater. Res. Bull.* **1980**, *15*, 671.

[30] J. Zou, C. Sole, N. E. Drewett, M. Velický, L. J. Hardwick, *J. Phys. Chem. Lett.* **2016**, *7*, 4291.

[31] G. Zhong, X. Wu, L. D'Arsie, K. B. K. Teo, N. L. Rupesinghe, A. Jouvray, J. Robertson, *Appl. Phys. Lett.* **2016**, *109*, 193103.

[32] M. V. L. Bennett, R. S. Zukin, *Neuron* **2004**, *41*, 495.

[33] a) J. T. Ye, Y. J. Zhang, R. Akashi, M. S. Bahramy, R. Arita, Y. Iwasa, *Science* **2012**, *338*, 1193; b) J. M. Lu, O. Zheliuk, I. Leermakers, N. F. Q. Yuan, U. Zeitler, K. T. Law, J. T. Ye, *Science* **2015**, *350*, 1353.

[34] Y. Ben-Ari, *Nat. Rev. Neurosci.* **2002**, *3*, 728.

[35] S. H. Choi, J. Kim, Y. S. Yoon, *J. Power Sources* **2004**, *138*, 283.

[36] J. S. Gnanaraj, R. W. Thompson, J. F. DiCarlo, K. M. Abraham, *J. Electrochem. Soc.* **2007**, *154*, A185.

[37] N. Kularatna, *IEEE Instrum. Meas. Mag.* **2011**, *14*, 20.

[38] V. V. Zhirnov, R. K. Cavin, S. Menzel, E. Linn, S. Schmelzer, D. Brauhaus, C. Schindler, R. Waser, *Proc. IEEE* **2010**, *98*, 2185.

[39] Z. Jiadi, Y. Yuchao, J. Rundong, L. Zhongxin, Z. Wen, R. Z. Ur, B. Lin, Z. Xiaoxian, C. Yimao, S. Li, H. Ru, *Adv. Mater.* **2018**, *30*, 1800195.